A SAR-GMTI Approach Aided by Online Knowledge With an Airborne Multichannel Quad-Pol Radar System

Chaolei Han , Zhiwei Yang, Guisheng Liao , *Senior Member, IEEE*, Qingjun Zhang, Shun He, and Huajian Xu

Abstract—In the complicated geographical environment, there will be a seriously deleterious effect to the performance of synthetic aperture radar (SAR)-ground moving target indication (SAR-GMTI) system, because it is difficult to obtain the homogeneous training samples to accurately estimate the clutter covariance matrix (CCM) without prior information of the observed scene. To this end, this article proposes a SAR-GMTI approach aided by online knowledge with an airborne multichannel quadrature-polarimetric (quad-pol) radar system. Generally, this article can be divided into two parts: online knowledge acquisition and polarization knowledge-aided (Pol-KA) SAR-GMTI processing. First, based on the similarity of pixels from the multichannel and multipolarization information, a weighed estimation method of polarimetric coherency matrix is proposed, which can overcome the over-smoothing problem and increase the estimation accuracy of coherency matrix. Furthermore, a hybrid weighted local K-means based on geodesic distance (GD-HWLKM) clustering algorithm is proposed to achieve the aim of unsupervised classification. Here, GD is exploited to measure the distance between multifeature region covariance matrixes (MFRCMs) and a hybrid weight from different scales (including local cover class distribution, region, and pixel) is calculated to automatically update the cluster centroid, which can make full use of the local spatial information by taking the interclass samples' similarity and the diversity of different classes into consideration. Second, with the assistance of the previous polarization SAR (PolSAR) image classification result, a Pol-KA SAR-GMTI method is developed. For each ground cover category, an accurate CCM can be estimated with the independent and identically distributed (IID) training samples. Then, the multichannel clutter suppression and preliminary constant false alarm rate (CFAR) detection are performed. Finally, with an airborne multichannel quad-pol radar system, the experimental results on real measured data demonstrate that the proposed method can efficiently improve the clutter suppression preformation and moving-target detection preformation.

Index Terms—Ground moving target indication (GMTI), online knowledge, quadrature-polarimetric (quad-pol) radar, synthetic aperture radar (SAR), weighted K-means clustering.

I. INTRODUCTION

WITH ensuring high-resolution, synthetic aperture radar (SAR)-ground moving target indication (SAR-GMTI) technology is capable of velocity estimation and localization of ground moving targets [1], [2]. In the actual environments, the ground moving targets usually are submerged in strong clutter. In order to reliably detect the moving targets, the azimuth multichannel methods are proposed, such as imaging space-time adaptive processing (ISTAP) [3], extended displaced phase center antenna (EDPCA) [4], and joint pixel vector processing [5]. The above-mentioned methods can obtain a satisfactory clutter suppression performance with a relatively accurate clutter covariance matrix (CCM) for the homogeneous clutter scene. But, in the actual work, the geographical environment observed is often complicated and the clutter distribution is inhomogeneous, such as sea-land, suburban or shadow-covered mountains. The traditional sample covariance matrix (SCM) method [6] ordinarily estimates the CCM by using the clutter samples from all distances. The power and distribution characteristics of training samples are always different with the range cell under test, which causes a significant reduction for the clutter suppression performance. The power selection training (PST) method [7] can solve the problem that the clutter suppression performance is insufficient by selecting the high power samples and can effectively suppress the strong clutter. However, this method certainly broadens the clutter adapting notch with the high-power samples, which will reduce the detection capability of the moving targets.

The prior knowledge-aided (KA) method is a possible way to circumvent this drawback by the prior environment information surrounding the radar [8], [9], [10], which selects representative training samples to construct the CCM aided by the digital terrain elevation models (DTEMs), the geographic information systems (GISs) and the land cover categories map. It can effectively suit inhomogeneous environment, but the timeliness of the prior

Chaolei Han is with the National Laboratory of Radar Signal Processing, Xidian University, Xi'an 710071, China (e-mail: hancl_xd@163.com).

Zhiwei Yang and Guisheng Liao are with the National Laboratory of Radar Signal Processing, Xidian University, Xi'an 710071, China, and also with the Collaborative Innovation Center of Information Sensing and Understanding, Xidian University, Xi'an 710071, China (e-mail: yangzw@xidian.edu.cn; liaogs@xidian.edu.cn).

Qingjun Zhang is with the China Academy of Space Technology, Beijing 100094, China (e-mail: qj_zhang@aliyun.com).

Shun He is with the Communication and Information Engineering Collage, Xi'an University of Science and Technology, Xi'an 710054, China (e-mail: heshun1212@163.com).

Huajian Xu is with the Nanjing Electronic Equipment Institute, Nanjing 210007, China (e-mail: huajianxu_xdrsp@126.com).

knowledge limits its widely application. In addition, system errors such as the platform's position error, attitude error, or beam pointing error may lead to the clutter mode of the recorded data mismatch with the prior knowledge, which will greatly reduce the estimation accuracy of CCM. However, the classification technology of polarimetric synthetic aperture radar (PolSAR) images can provide the online geographic or land cover information to help to robustly estimate CCMs in SAR-GMTI processing for the relatively identical clutter categories.

The clutter classification techniques contain supervised classification [11], [12], [13], [14], semisupervised classification [15], [16], [17], [18], and unsupervised classification [19], [20], [21], [22], [23], [24]. However, for SAR-GMTI processing, the mismatch between the land cover categories of the recorded data and the prior knowledge usually occurs because of the inevitable system errors, which make it difficult to obtain the labeled training samples. Therefore, the unsupervised classification methods are the most appropriate approaches to help to improve the SAR-GMTI processing performance. The unsupervised methods usually represent the inner structure information of unlabeled data by designing a function and make a decision rule to cluster samples into several different groups. Without any prior knowledge, the unsupervised methods have been widely considered, such as Wishart classifier [19], Markov random field methods [20], [21], polarimetric scattering characteristic-preserved method [22], K-means cluster classifier [23], fuzzy c-means cluster classifier [24], and so on. Owing to the simplicity of operation and small computational complexity, K-means clustering approach has become one of the most popular PolSAR image classification methods, which can be applied to improve the preformation of the actual SAR-GMTI systems in the increasingly diverse surveillance tasks.

The K-means approach is an iterative optimization algorithm, which mainly is related to three aspects: the representation of samples, the distance metric between unlabeled samples and the cluster centroids, and the updated mode of cluster centroids, as follows: 1) is the representation of samples. In fact, not only for the K-means approaches, the representation of samples is usually an important factor to the great mass of PolSAR classification methods. The classical representation way is based on pixels. Lee et al. [25] classify the PolSAR image pixels using K-means algorithm with the multivariate complex Wishart distribution of sample coherency matrices. Chen et al. [26] achieve PolSAR image unsupervised classification based on the scattering similarity between pixels. Bi et al. [27] also propose an unsupervised PolSAR image classification using discriminative clustering. But, the pixel-based classification methods are easily affected by the speckle noise. Recently, region covariance-based classification has been widely applied to PolSAR image classification [28], [29]. As one type of representation of samples, region covariance matrix (RCM) considers the relation between neighbor pixels and can efficiently suppress the speckle noise. Besides, compared with the pixel vector, RCM-based representation can take the correlated properties of features into account by providing both the variance of each feature (i.e., matrix's diagonal entries) as well as the joint distribution between them (i.e., matrix's off-diagonal entries). 2) is the distance metric between unlabeled
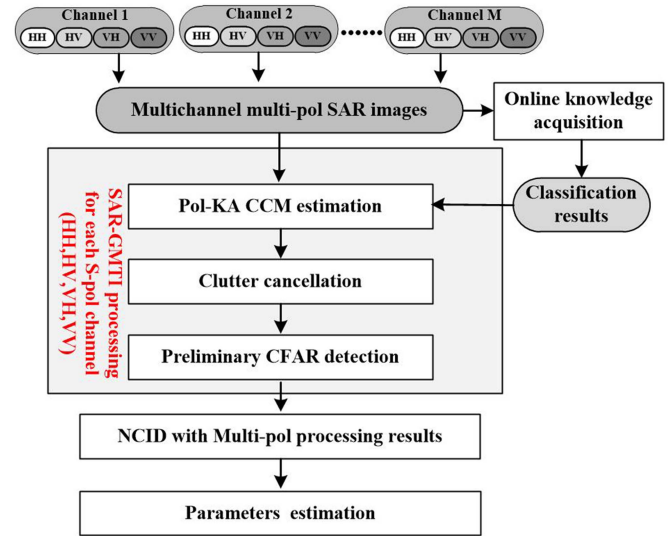

Fig. 1. Framework of the proposed method, where it has M spatial channels for each polarimetric component (HH, HV, VH, and VV).

samples and the cluster centroids. The classical or standard distance metric is norm-based metric, including Euclidean distance [30], Manhattan distance [31], log-Euclidean distance [32], and so on. Furthermore, the Wishart-based [23] dissimilarity measure has become a popular distance metric. Song et al. [33] adopt the Bartlett distance to replace the similarity measure in PolSAR classification tasks. Kersten et al. [24] have identified that the distance measures based on the Wishart distribution have a better unsupervised classification performance than those based on the norms. In the past few years, scholars find that the covariance matrices with semipositive definite structure do not lie on the Euclidean space but on the Riemannian space. So, the affine invariant Riemannian (AIR) distance [29], [34] is proposed to define the distance between covariance matrices. But, the AIR distance requires eigenvalue decomposition operation and has a high computation complexity. 3) is the updated mode of cluster centroids. The standard K-means algorithm equally treats all variables and do not select samples in the clustering process, which usually cannot obtain a satisfactory result. Many works about variable weighted clustering have been progressed to improve the performance by identifying important variables with variable weights [35], [36]. This updated mode of cluster centroids can be seen as feature extraction. Xiang et al. [37] update the cluster centroids with a weighted local K-means algorithm by measuring the similarity of pixels, which can improve the clustering result but it is easily affected by the speckle noise. In addition, the aforementioned PolSAR image classification methods are based on the PolSAR systems with one azimuth receive channel.

This article mainly pays attention to improve SAR-GMTI performance aided by online PolSAR image classification knowledge with the multipolarization and multichannel SAR-GMTI system. As shown in Fig. 1, this article mainly can be divided into two parts: online knowledge acquisition by the proposed hybrid weighted local K-means based on geodesic distance (GD-HWLKM) clustering algorithm and online polarization

knowledge-aided (Pol-KA) SAR-GMTI processing. In part I, we first propose a weighed estimation method of coherency matrix for multichannel PolSAR system to robustly estimate the polarimetric coherency matrix, which can overcome the over-smoothing problem and increase the estimation accuracy of coherency matrix by effectively taking advantage of the multichannel and multipolarization information. Then, the significant polarimetric features belonging to different categories are extracted with multifeature RCM (MFRCM), including the polarimetric decomposition-based, color, and texture features. Different from the existing feature selection methods, we extract the texture features from the scattering model-based decomposition features map, which can represent the structure of different physical scattering components better. Due to the MFRCMs lie on the Riemannian space, GD [38], [39] is exploited to describe the similarity distance between them, which can effectively tolerate the scaling and rotation between MFRCMs. And, we also discuss other distance metrics. Furthermore, to achieve the aim of unsupervised classification, a GD-HWLKM clustering algorithm is proposed within the K-means algorithm framework. Where the hybrid weight is calculated to describe the interclass samples' similarity and the diversity of different classes from different scales, including local cover class distribution, region, and pixel, which can make full use of the local spatial information and can preserve the edges as many as possible. In part II, an online Pol-KA SAR-GMTI processing method is developed with the assistance of the previous Pol-SAR image classification results. For each single-polarimetric (S-pol) component, the independent and identically distributed (IID) clutter training samples are selected to accurately estimate the CCM of each land cover. Then, the clutter cancellation in image domain for each land cover and preliminary constant false alarm rate (CFAR) detection are performed. Besides, the noncoherence integration detection (NCID) technique is exploited to reduce the false alarms, further. Finally, the parameters estimation step is carried out to obtain the velocity of moving targets.

The main contributions of this article are listed as follows.

1) The proposed weighed estimation method of coherency matrix not only can reduce the effect of speckle noise when solving the over-smoothing problem, but also can increase the estimation accuracy of coherency matrix by the local weight based on the similarity of pixels from the multichannel and multipolarimetric information.

2) The proposed unsupervised GD-HWLKM PolSAR image clustering approach can achieve a better classification performance while preserving the edges. This algorithm first utilizes GD to measure the distance between MFR-CMs, which is more effective for classification. Meanwhile, considering the interclass samples' similarity and the diversity of different classes, a hybrid local weight is constructed to revise the KM algorithm from different scales, which can preserve the image edges and obtain the better classification result.

3) An online Pol-KA SAR-GMTI method is developed based on the airborne multichannel quad-pol radar system. Under the guidance of the online knowledge about the land
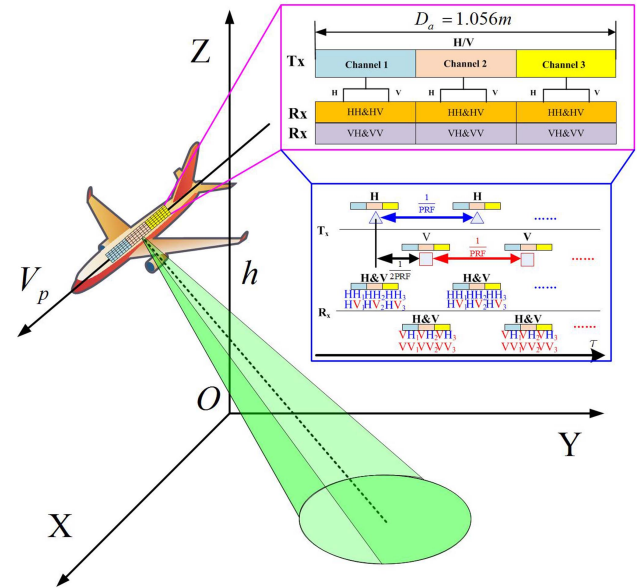

Fig. 2. Schematic of operation mode for quad-pol radar system with multiple azimuth receiving channels.

scene, the IID clutter samples are selected to accurately estimate CCM for each land cover, which can improve clutter suppression and moving-target detection performance.

The rest of this article is organized as follows. Section II gives an introduction about the operation of airborne multichannel quad-PolSAR systems. In Section III, the proposed method is described in detail. And the experiment results based on the real measured data are presented in Section IV. Finally, Section V concludes this article.

II. OPERATION OF AIRBORNE MULTICHANNEL QUAD-PolSAR SYSTEM

Since the multichannel and multipolarization data are used in this article, the quad-pol airborne radar system with multiple azimuth receiving channels is brief introduced as follows: As shown in Fig. 2, the airborne quad-pol radar system [40] operates in side-looking mode with platform velocity V_p, platform height h, including three azimuth receiving channels. The H- and V-polarization echoes can be simultaneously received for each azimuth receiving channel. H-polarization channel transmits the horizontally polarized radar pulses with azimuth full aperture D_a and three spatial receiving channels receive the returns with H polarization and V polarization, simultaneously, which can form the HH and HV polarization components. Similarly, the VH and VV components are formed when V-polarization channel transmits the vertically polarized radar pulses. Then, HH-pol, HV-pol, VH-pol, and VV-pol components of each azimuth receiving channels are performed SAR image processing to obtain the multichannel and multipolarization SAR images.

III. METHODOLOGY

The framework of the proposed method can be seen in Fig. 1. This article mainly can be divided into two parts: online

knowledge acquisition and Pol-KA GMTI processing. First, the online Pol-KA GMTI processing aided by polarimetric classification result is developed. Second, online knowledge acquisition is given in detail, which contains three main stages including the weighed estimation of coherency matrix with the multichannel SAR system, the multiple feature extraction with RCMs, and the unsupervised classification by the proposed GD-HWLKM clustering algorithm. We now describe them in detail.

A. Multichannel SAR-GMTI Processing Aided by Online Polarimetric Classification Knowledge

1) Signal Model and Traditional CCM Estimation Method:
In multichannel GMTI processing, the detection for the pth pixel in image domain can be expressed as follows:

$$H_0 : \boldsymbol{x}(p) = \boldsymbol{c}(p) + \boldsymbol{n}(p)$$
$$H_1 : \boldsymbol{x}(p) = \gamma_p \cdot \boldsymbol{s}(p) + \boldsymbol{c}(p) + \boldsymbol{n}(p) \tag{1}$$

where $\boldsymbol{x}(p) \in \mathbb{C}^{M \times 1}, \boldsymbol{s}(p) \in \mathbb{C}^{M \times 1} \boldsymbol{c}(p) \in \mathbb{C}^{M \times 1}$, and $\boldsymbol{n}(p) \in \mathbb{C}^{M \times 1}$ represent the pixel data vector, moving-target signal vector, clutter vector, and noise vector, respectively. γ_p denotes the complex amplitude of target and M is the number of spatial receiving channel.

To suppress the clutter, the optimal weight calculation is given in image domain by the linear constraint minimum variance (LCMV) criterion

$$\begin{cases} \min_{\boldsymbol{w}} \; \boldsymbol{w}^H(v_r) \, \boldsymbol{R}_{cn} \boldsymbol{w}(v_r) \\ s.t \quad \boldsymbol{w}^H(v_r) \, \boldsymbol{s}(v_r) = 1 \end{cases} \tag{2}$$

where $[\cdot]^H$ represents the conjugate transpose operation, $\boldsymbol{s}(v_r)$ is the multichannel spatial steering vectors of moving-target with the radial velocity v_r, $\boldsymbol{w}$ is the optimum weight, and $\boldsymbol{R}_{cn}$ is the ideal CCM of the RCUT. Obviously, the CCM $\boldsymbol{R}_{cn}$ of the RCUT only can be obtained by estimating. And, the well-known Reed–Mallett–Brennan (RMB) rule [6] has proved that it requires the IID training samples and can achieve an averaging performance loss within 3 decibels (dB). In the traditional CCM estimation method [3], [4], [5], the CCM is estimated by the pixel data vectors of adjoining range cells, which are regarded as training samples, as follows:

$$\hat{\boldsymbol{R}}_{cn} = \frac{1}{K} \sum_{k=1}^{K} \boldsymbol{x}(k) \boldsymbol{x}(k)^H \tag{3}$$

where $\hat{\boldsymbol{R}}_{cn}$ is the estimation of $\boldsymbol{R}_{cn}$ with traditional methods and K is the number of training samples.

2) Proposed Online Pol-KA SAR-GMTI Method: In the complicated observation environment, the various land covers usually have different clutter scattering and statistic characteristics, which often result in severe performance degradation of the traditional methods. To this end, it is a core issue to estimate CCMs by selecting the homogeneous training samples for achieving a great GMTI performance.

In this article, an online Pol-KA SAR-GMTI method is developed with the guidance of polarimetric classification. The accurate CCM for each land cover can be estimated with the

clutter samples belonging to the same cover category, which have the same scattering characteristic and can be regarded as homogeneous clutter and generally satisfy IID, as follows:

$$\hat{\boldsymbol{R}}_{cn}(1) = \sum_{k \in C_1} \eta_1 \cdot \boldsymbol{x}(k) \boldsymbol{x}(k)^H$$

$$\hat{\boldsymbol{R}}_{cn}(2) = \sum_{k \in C_2} \eta_2 \cdot \boldsymbol{x}(k) \boldsymbol{x}(k)^H$$

$$\vdots$$

$$\hat{\boldsymbol{R}}_{cn}(L) = \sum_{k \in C_L} \eta_L \cdot \boldsymbol{x}(k) \boldsymbol{x}(k)^H \tag{4}$$

where $\hat{\boldsymbol{R}}_{cn}(l)$ is the estimation value of $\boldsymbol{R}_{cn}$ by the proposed method for the lth $(l = 1, 2, \cdots, L)$ land cover category, C_l is the lth clutter samples dataset from the online polarimetric classification result, $k \in C_l$ represents the training samples belonging to C_l. η_l denotes a weighting real coefficient of samples data for the lth land cover from polarimetric classification result, which satisfies $\eta_l = 1/N_l$ and N_l is the number of lth land cover clutter samples dataset.

After obtaining the CCM of each land cover, the optimum weight $\boldsymbol{w}_{opt}(v_r) = \frac{\hat{\boldsymbol{R}}_{cn}^{-1} \boldsymbol{s}(v_r)}{\boldsymbol{s}^H(v_r) \hat{\boldsymbol{R}}_{cn} \boldsymbol{s}(v_r)}$ can be employed to suppress the clutter. The detection performance is directly proportional to the output signal-to-clutter-plus-noise ratio (SCNR) at the output of the adaptive matched filter for clutter suppression, which can be calculated as follows:

$$SCNR = \frac{\boldsymbol{w}_{opt}^H \boldsymbol{R}_s \boldsymbol{w}_{opt}}{\boldsymbol{w}_{opt}^H \hat{\boldsymbol{R}}_{cn}(l) \, \boldsymbol{w}_{opt}} \tag{5}$$

where $\boldsymbol{R}_s$ is the multichannel data matrix of the moving target.

Different from the KA methods [8], [9], [10], the proposed method is more suitable to the inhomogeneous environment without any prior knowledge. In the KA methods, CCM is estimated with $\hat{\boldsymbol{R}}_{KA} = \zeta \cdot \boldsymbol{R}_0 + (1 - \zeta) \cdot \hat{\boldsymbol{R}}_{cn}$, where $\hat{\boldsymbol{R}}_{cn}$ is the estimation value of CCM in (3), $\boldsymbol{R}_0$ is the constructed CCM by exploited the knowledge of radar, and ζ is the weight coefficient. Evidently, the proposed method is entirely based on the receiving data, which can absolutely suit the system working state and avoid the mismatch between the prior knowledge and the receiving data. And, it can be widely applied to the complicated environment, such as sea-land, suburban, urban, shadow-covered mountains, and so on. In summary, the proposed method can obtain the accurate estimation values of CCM for each ground cover under the guidance of the obtained online classification knowledge. Therefore, the online knowledge acquisition suiting the multichannel and multipolarimetric system is the research focus for the next article.

B. Weighed Estimation Method of Coherency Matrix

As a major polarimetric carrier, the estimation of coherency matrix is a fatal step for the PolSAR images classification. Traditionally, an averaging operator is used to perform the spatial multilook processing to reduce the effect of speckle noise. But, this averaging filter will unavoidably cause the over-smoothing

problem and debase the accuracy of the estimated coherency matrix. To address this problem, in this article, we propose a weighed estimation method of coherency matrix for multichannel PolSAR system.

As we all know, the multichannel data are the reflection echoes obtained from the radar at the same time and the same scene. So, there is only a little difference for an arbitrary receiving channel relative to the reference channel, which is mainly reflected in correlation coefficient (or interferometric phase). The bigger correlation coefficient is; the more similar coherence matrixes are. In this article, we propose to fuse the coherency matrixes from different receiving channels by weighted estimation with correlation coefficients between channels. This step can be seen as a multilook operation among channels, as follows:

$$T_p = \frac{1}{\sum_{m=1}^{M} \rho_{r,m}} \left[\sum_{m=1}^{M} \rho_{r,m} \cdot (T_p)_m \right] \tag{6}$$

where $(T_p)_m$ is the estimated coherency matrix of the pth pixel with mth receiving channel, $\rho_{r,m}$ represents the correlation coefficient between rth and mth channels, which can be calculated in [41]. Here, it should be noted that we generally assume the rth receiving channel is the reference channel and the correlation coefficient is equal to 1 when $m = r$.

For coherency matrix of each receiving channel, we not only consider the pixel similarity of polarimetric, but also take the interferometric phase information between channels into consideration by a pixel similarity weight during multilook procedure. If the pixels are more similar, their similarity weight will be bigger. For the mth spatial receiving channel, the weighted coherency matrix for the pth pixel can be estimated as follows:

$$(T_p)_m = \frac{1}{\sum_{q \in N_p} \omega_p(q)} \sum_{q \in N_p} \omega_p(q) \boldsymbol{k}_q \boldsymbol{k}_q^T \tag{7}$$

where
1) N_p represents the neighborhood around pixel p.
2) $\boldsymbol{k}$ is the complex polarinetric scattering vector in Pauli representation in the mth receiving channel, as follows:

$$\boldsymbol{k} = \frac{1}{\sqrt{2}}[S_{hh} - S_{vv}, 2S_{hv}, S_{hh} - S_{vv}]^T. \tag{8}$$

3) $\omega_p(q)$ is the similarity weight of qth pixel inside the neighborhood N_p, which is defined as follows:

$$\omega_p(q) = \exp\left\{ -\frac{d^2(p,q)}{\sigma_p^2} \right\} \tag{9}$$

where $d(p,q) = \|\boldsymbol{g}_p - \boldsymbol{g}_q\|_2$ involves a dissimilarity measure between pixel p and q. and $\boldsymbol{g} = [\boldsymbol{k}_1^T, \boldsymbol{k}_2^T, \cdots \boldsymbol{k}_M^T]^T$ is the multichannel and multipolarimetric united data vector. It should be noted that the interferometric phase information between channels also is taken into account different with the traditional method, which can robustly measure the similarity of pixels in neighborhood. $\sigma_p = \sqrt{\pi/2}\text{MAD}$ is the scale parameter, which can be estimated by the mean absolute deviation (MAD) [42] of all the distance value $d(p,q), \forall q \in N_p$.
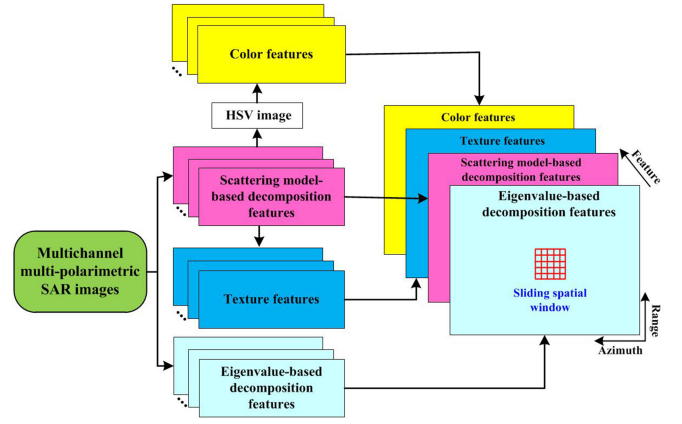

Fig. 3. Multifeature representation of data. The region is built with a sliding spatial window for each pixel.

C. Feature Extraction With Multifeature RCM

It is obvious that the features based on the decomposition theories are just linear transformations from the original polarimetric features (including the complex scattering matrix, covariance matrix, coherency matrix elements, and so on). So, for reducing feature redundancies, the features based on the different decomposition theories are only considered to extract the polarimetric scattering information. Besides, different from the existing methods, the texture features are extracted from the scattering model-based decomposition features map in this article, which can describe the structure of different physical scattering components better. As shown in Fig. 3, the extracted PolSAR features can generally be divided into two different categories: polarimetric features and the spatial structure features.

1) belongs to the polarimetric features usually based on the different decomposition theories, which try to describe the average scattering power by some independent components. In this article, scattering model-based decomposition (Yamaguchi decomposition) [43] and eigenvalue-based decomposition (H/A/α decomposition) [44] are exploited to extract the polarimetric features. The Yamaguchi decomposition features can be formed as $\boldsymbol{f}_{Yama} = [P_s, P_d, P_v, P_h]^T$, where P_s, P_d, P_v, and P_h represent the scattering power of surface, double-bounce, volume, and helix scatterings, respectively. The eigenvalue-based decomposition features are formed as $\boldsymbol{f}_{Eigen} = [H, A, \alpha]^T$, where H, A, and α are the scattering entropy, anisotropy, and alpha angle, respectively.

2) can be regarded as the spatial structure features, such as color features [45] and texture features [34]. In this article, the image gradients are utilized to represent the texture features with $\boldsymbol{f}_{Texture} = [\boldsymbol{f}_{Texture}^s, \boldsymbol{f}_{Texture}^d, \boldsymbol{f}_{Texture}^v, \boldsymbol{f}_{Texture}^h]^T$ where $\boldsymbol{f}_{Texture}^s$, $\boldsymbol{f}_{Texture}^d$, $\boldsymbol{f}_{Texture}^v$, $\boldsymbol{f}_{Texture}^h$ are the texture features extracted from the surface, double-bounce, volume and helix scattering power maps, respectively. And, $\boldsymbol{f}_{Texture}^{i,i\in\{s,d,s,v\}} = [I_{xx}^i, I_{xy}^i, I_{yx}^i, I_{yy}^i]$ is the gradient of different direction, where $I_{xx}^i, I_{xy}^i, I_{yx}^i, I_{yy}^i$ are the horizontal-, cross- and vertical-gradients, respectively.

TABLE I
EXTRACTED FEATURES

| Features	Features
P_s, P_d, P_v, P_h	Scattering model-based decomposition
H, A, α	Eigenvalue-based decomposition
$\boldsymbol{f}^s_{Texture}, \boldsymbol{f}^d_{Texture}, \boldsymbol{f}^v_{Texture}, \boldsymbol{f}^h_{Texture}$	Texture
$h_1, h_2, \ldots, h_7, s_1, s_2, s_3, v_1, v_2, v_3$	Color

Fig. 4. Construction of the proposed hybrid weighted local K-means clustering algorithm based on GD of MFRCMs. The local class distribution-based weight describes the class's similarity of all pixels in neighborhood regions, the region-based weight describes the similarity of neighborhood regions, and the pixel-based weight describes the similarity of pixels in current region.

They are calculated using mean ratio operator [46]. It should be noted that the gradients are extracted with scattering model-based decomposition feature images of PolSAR but not with original images, which can take advantage of spatial and polarimetric features as much as possible. In addition, the color features are sufficiently represented by the color histograms to describe the color distributions for each pixel, which can commendably adapt to the human eye system. Detailedly, for each pixel, we use a local sliding window to select the neighborhood pixels and count the number of pixel belonging to each color level. In this article, the RGB image is first composited with the double-bounce scattering (red), volume scattering (green) and surface scattering (blue). Then, according to the human vision, this RGB image is converted to the hue-saturation-value (HSV) images, which contain 7, 3 and 3 color levels of the hue, saturation and value, respectively. Therefore, the color features contain 13 bins, as $\boldsymbol{f}_{Color} = [h_1, h_2, \ldots, h_7, s_1, s_2, s_3, v_1, v_2, v_3]^T$, where h_i, s_i and v_i is the hue, saturation, value bin, respectively. For normalization, all features can be linearly into $[-1, 1]$.

In a word, this article extracts multiple significant features are listed in Table I.

As a local feature descriptor, RCM considers the relation between neighbor pixels and can efficiently suppress the speckle noise. Besides, compared with the pixel feature vector, RCM can take into account their correlated properties by providing both the variance of each feature and their joint distribution. We first construct the feature vector with earlier multiple features to describe the scattering characteristics and local spatial structure of each pixel, as follows:

$$\boldsymbol{f}_p = \left[\boldsymbol{f}^T_{Yama}, \boldsymbol{f}^T_{Eigen}, \boldsymbol{f}^T_{Texture}, \boldsymbol{f}^T_{Color} \right]^T. \quad (10)$$

Assuming that a local image region is constructed by $w \times w$ pixels around a studied pixel $p \in I$, which is denoted by $\mathcal{N}(p)$ and built from a sliding spatial window. The MFRCM is defined as follows:

$$\boldsymbol{R}_p = \frac{1}{w^2} \sum_{q \in \mathcal{N}(p)} \left(\boldsymbol{f}_q - \boldsymbol{\mu} \right) \left(\boldsymbol{f}_q - \boldsymbol{\mu} \right)^T \quad (11)$$

where $\boldsymbol{f}_q \in \mathbb{R}^{36}$ is the multifeature vector at pixel q. $\boldsymbol{\mu} = (1/w^2) \sum_{q \in \mathcal{N}(p)} \boldsymbol{f}_q$ represents the estimated mean value of the
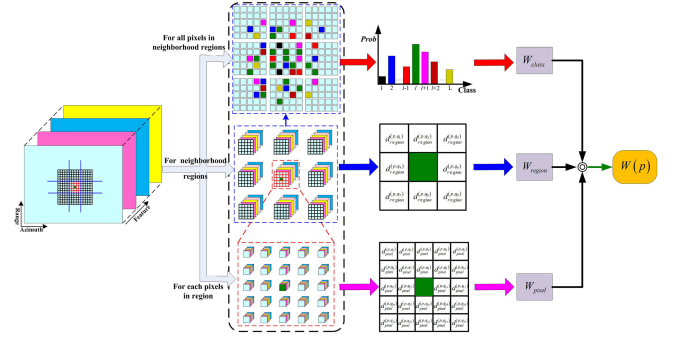
multifeature vector with local region $\mathcal{N}(p)$. Obviously, the RCM is a local polarimetric-geometric descriptor including multiple features. In addition, it should be noted that the used feature descriptor is not limited to only contain the above-mentioned four different features and the other useful features also can be incorporated into this descriptor.

D. Proposed Hybrid Weighted Local K-Means Clustering Algorithm Based on GD of MFRCMs

The weighted K-means clustering is an effective unsupervised algorithm, which has a relatively small computational complexity and has been widely applied in PolSAR image classification tasks. Traditionally, the weighted K-means clustering algorithms mainly focus on the weight with pixel feature vector representation, which cannot capture the local spatial information. Although the RCM-based methods partly overcome this shortcoming by using the RCM representation, there are still two important issues. On the one hand, the traditional methods usually utilize norm distance or Wishart distances to describe the similarity of MFRCMs, which cannot tolerate the scaling and rotation of MFRCMs. On the other hand, they only calculate the weights with single scale (region) samples and completely ignore the diversity among pixels with the assumption that all pixels from each local region belong to the same class, which will lose a great deal of structure information, such as edges. To address these issues, a GD-HWLKM PolSAR image clustering algorithm is proposed in this article. First, GD is exploited to describe the similarity of MFRCMs because they lie on the Riemannian space, which can effectively tolerate the scaling and rotation of MFRCMs. Furthermore, it is clearly that the homogeneous points should be the more believable than the inhomogeneous points that are generally located in the edge areas or heterogeneous areas. As shown in Fig. 4, three different types of weights from different scales are taken into consideration to measure the local distribution characteristics, including: 1) local class distribution-based weight (large scale), 2) region-based weight (medium scale), and 3) pixel-based weight (small scale). The constructed hybrid weight can preserve the local structure information as much as possible by the restriction in different

scales. The details of the proposed GD-HWLKM algorithm are presented as follows.

Let c_l be the lth $(l = 1, 2, \ldots, L)$ cluster and L be the total class number. The MFRCM of point p is $\boldsymbol{R}_p$, then the objective function F_{KM} of the proposed weighted K-means is defined as follows:

$$F_{KM} = \sum_{l=1}^{L} \sum_{p \in c_l} W(p) \left(D_{GD} \left(\boldsymbol{R}_p, \widehat{\boldsymbol{R}}_l \right) \right)^2 \qquad (12)$$

$$\widehat{\boldsymbol{R}}_l = \frac{\sum_{q \in c_l} W(q) \boldsymbol{R}_q}{\sum_{q \in c_l} W(q)} \qquad (13)$$

where $\widehat{\boldsymbol{R}}_l$ represents the lth cluster centroid, which can enhance the discrimination by using RCM descriptor and GD metric. c_l is the lth class dataset. $D_{GD}(\boldsymbol{R}_p, \widehat{\boldsymbol{R}}_l)$ is the GD between the pth point and the lth cluster centroid, which is defined as follows [38], [39]:

$$D_{GD} \left(\boldsymbol{R}_p, \widehat{\boldsymbol{R}}_l \right) = \frac{2}{\pi} \cos^{-1} \frac{Tr \left(\boldsymbol{R}_p^T \widehat{\boldsymbol{R}}_l \right)}{\sqrt{Tr \left(\boldsymbol{R}_p^T \boldsymbol{R}_p \right)} \sqrt{Tr \left(\widehat{\boldsymbol{R}}_l^T \widehat{\boldsymbol{R}}_l \right)}} \qquad (14)$$

where $(\cdot)^T$ and $Tr(\cdot)$ donate the transpose and trace operators, respectively. $W(p)$ is the assigned hybrid weight for the pth point, as shown in Fig. 4, which is composed of three types of weights from different scales. The construction details of them are presented as follows.

1) Local Class Distribution-Based Weight: In the homogeneous areas, the pixel classes are usually alike. On the contrary, the pixel classes should be diverse in the heterogeneous areas. Therefore, in each iteration, the local class (or clutter type) diversity from the temporary classification can represent the local spatial information, which can be regarded as the large-scale information. In this article, we use the class distribution probability to represent this local spatial information. Assume that the class of current pixel is $l_p \in 1, 2, \ldots, L$, the local class distribution-based weight is defined as follows:

$$W_{class}(p) = \frac{Num(class = l_p)}{\sum_{l=1}^{L} Num(class = l)} \qquad (15)$$

where $Num(class = l)$ represents the total number of pixel-based points belonging to the lth clutter type. Obviously, in this large scale, the local class distribution is more concentrated on the class of current pixel, the weighted value will be bigger and the current pixel is more believable to update the cluster centroids.

2) Region-Based Weight: The region-based weight is constructed by the spatial adjacency regions from the local image patches. It can be regarded as a medium-scale weight. The pth region is represented by the MFRCM $\boldsymbol{R}_p$. Let $\boldsymbol{R}_{\mathcal{N}} = \{\boldsymbol{R}_1, \boldsymbol{R}_2, \ldots, \boldsymbol{R}_q, \ldots, \boldsymbol{R}_Q\}$ denote the spatial adjacency regions. And, the region-based weight $W_{region}(p)$ is defined as follows:

$$W_{region}(p) = \frac{1}{N_{l_q=l_p}^R} \sum_{\substack{\boldsymbol{R}_q \in \boldsymbol{R}_{\mathcal{N}} \\ l_q = l_p}} (1 - D_{GD}(\boldsymbol{R}_p, \boldsymbol{R}_q))$$

$$+ \left\{ \frac{1}{N_{l_q \neq l_p}^R} \sum_{\substack{\boldsymbol{R}_q \in \boldsymbol{R}_{\mathcal{N}} \\ l_q \neq l_p}} (D_{GD}(\boldsymbol{R}_p, \boldsymbol{R}_q)) \right\} \qquad (16)$$

where $\boldsymbol{R}_q$ is MFRCM of the qth adjacency region and Q is the total number of the spatial adjacency regions. It should be noted that $\boldsymbol{R}_q$ and $\boldsymbol{R}_p$ are adjoining but they do not have the same pixel, as shown in Fig. 4. For the same classes, the local regions are more similar, the region-based weight is bigger. And this local region will be more probably regarded as a homogeneous region. Conversely, the region-based weight will be close to 0. It should be noted that we define the first term or the second term is equal to zero in the above-mentioned formula when $N_{l_q=l_p}^R = 0$ or $N_{l_q \neq l_p}^R = 0$, respectively.

3) Pixel-Based Weight: For each MFRCM, all pixels belonging to a local patch are regarded as the same class, which ignore the diversity among pixels and might smooth the image edges. To address this issue, we construct a pixel-based weight to measure this diversity characteristic for each patch, which can be regarded as the least scale weight. From Section III.B, a local region $\mathcal{N}(p)$ contains $w \times w$ pixels around a studied pixel $p \in I$. The pixel-based weight is constructed as follows:

$$W_{pixel}(p) = \frac{1}{N_{l_q=l_p}} \sum_{\substack{q \in \mathcal{N}(p) \\ l_q=l_p}} \frac{1}{2} \cdot [1 + d_{pixel}(p, q)]$$

$$+ \frac{1}{N_{l_q \neq l_p}} \sum_{\substack{q \in \mathcal{N}(p) \\ l_q \neq l_p}} \frac{1}{2} \cdot [1 - d_{pixel}(p, q)] \qquad (17)$$

where $\boldsymbol{f}_q$ is the multifeature vector at pixel q. $d_{pixel}(p, q)$ is a similarity metric between two vectors, which is defined with the cosine value of vectors angle, as follows:

$$d_{pixel}(p, q) = \frac{\langle \boldsymbol{f}_p, \boldsymbol{f}_q \rangle}{\|\boldsymbol{f}_p\|_2 \cdot \|\boldsymbol{f}_q\|_2} \qquad (18)$$

where $\|\cdot\|_2$ is norm operation for vectors, $\langle \cdot \rangle$ is the operation for calculating the inner product between vectors. Obviously, the defined similarity metric also can tolerate the scaling and rotation of vectors, which is more reasonable and effective for measuring the similarity of different land covers owning various polarimetric information. Similarly, the first term or the second term is equal to zero in the above-mentioned formula when $N_{l_q=l_p}^R = 0$ or $N_{l_q \neq l_p}^R = 0$, respectively.

In summary, the local hybrid weight can be calculated with the above-mentioned three type weights, as follows:

$$W(p) = W_{class}(p) \cdot W_{region}(p) \cdot W_{pixel}(p) \qquad (19)$$

where it should be note that the above-mentioned weights are all performed by normalization operation in advance.

Algorithm 1: Proposed SAR-GMTI Approach.

Inputs: Multichannel and multipolarization image data.
The maximum number T, total class number L of covers and clustering end marker ε.

1: Online knowledge acquisition.

  1.1: Calculate the coherence matrixes by (6) and (7).

  1.2: Extract multiple features listed in Table I with MFRCM.

  1.3: Initial labels of covers and obtain the cluster centroids.

  1.4: **for** $t = 1$: T **do**

  1.5: Calculate local hybrid weight $W(p)$ by (19).

  1.6: Calculate objective function $F_{KM}(t)$ by (12).

  1.7: Update the cluster centroids by (13).

  1.8: Clustering by the GD between MFRCMs of samples and the cluster centroids by (14).

  1.9: **If** $t > 1$ and $|F_{KM}(t+1) - F_{KM}(t)| < \varepsilon$, **break**

  1.10: end for

2: Pol-KA GMTI processing.

  2.1: **for** HH-, HV-, VH-, and VV-pol component **do**

  2.2: Select the IID training clutter samples to estimate CCM by (4) for each type cover, respectively

  2.3: Calculate the optimal adaptive weight vector $\boldsymbol{w}_{opt}$ for each type cover by (2).

  2.4: Perform multichannel clutter suppression processing for each type cover using the corresponding $\boldsymbol{w}_{opt}$.

  2.5: Perform CFAR detection.

  2.6: end for

  2.7: Integrate the detection results of four polarimetric components by NCID technique.

  2.8: Perform radial velocity estimation of potential moving targets.

  Outputs: GMTI processing results

We first adopt the polarization-space classification technique [47] to obtain the initial cluster centroids. By alternately computing cluster centroid and performing the clustering steps, the above-mentioned function can be minimized with the iterative processing. In each iterative procedure, the weight value of each point will be updated with new cluster result. The proposed SAR-GMTI approach is summarized in Algorithm 1.

IV. EXPERIMENTAL RESULT AND ANALYSIS

In this section, the experiments on real measured data are performed to evaluate the proposed method. Section IV.A gives a brief description of the experimental data and Section IV.B is the experimental results, which is composed of the weighed estimation result of coherency matrix, the classification result of PolSAR image, and the GMTI processing result.

A. Data Description

The experimental multichannel and multipolarization data used in this article are taken by the quad-pol radar system with three azimuth receiving channels which operates at X-band (10

Fig. 5. Observation geometry of radar and illuminated scene, where optics images were from Google Earth on August 13, 2018, and the HH-pol amplitude SAR image, which overlaps on Google Earth optics image, was acquired by the airborne radar system, in April 2017.
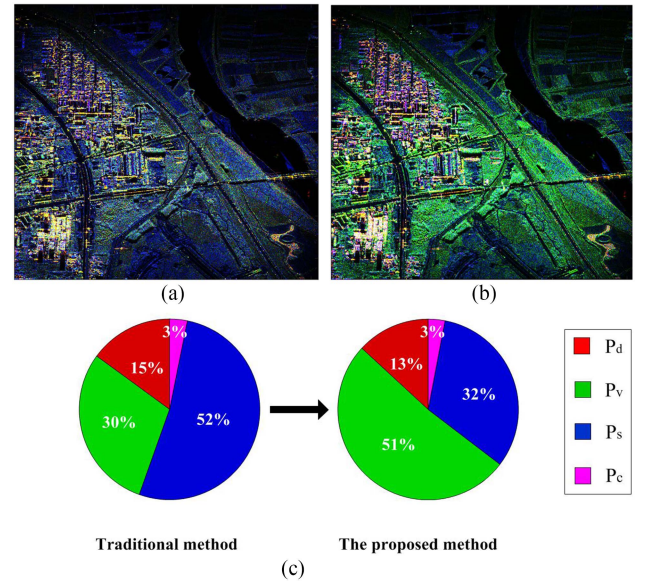

Fig. 6. False color image based on Yamaguchi decomposition. Red: double-bounce scattering, green: volume scattering, and blue: surface scattering. (a) False color image from the traditional estimated coherency matrix. (b) False color image from the proposed weighed estimated coherency matrix. (c) Power contribution of different scatterings.

GHz), platform height is 8000 m, antenna azimuth aperture is 1.056 m, the platform velocity is 150 m/s, and PRF is 800 Hz. The tested scene is located in Weinan, Shaanxi Province, China, in April 2017. In Fig. 5, we can see that this experimental scene is situated in the northeast of Weinan city and adjacent to the Weihe river. The single-look slant-range and the azimuth resolutions are about 0.5 m for the experimental data. For reducing processing time, the azimuth resolution is reduced to 2 m by multilook
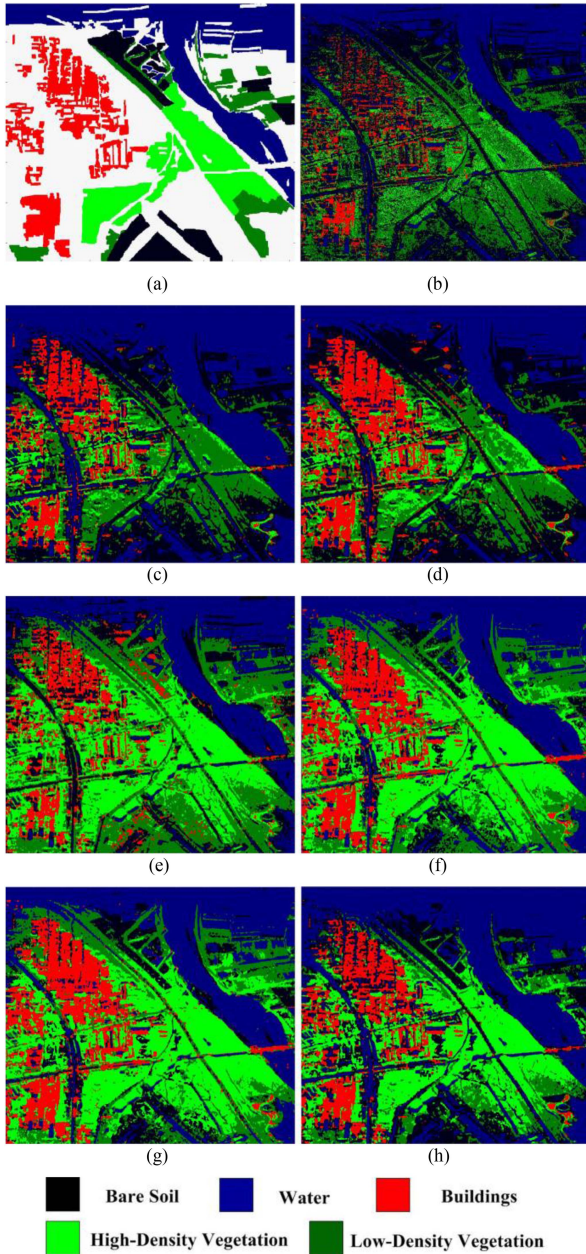
Fig. 7. Classification results by K-mean algorithm with different distance metrics. (a) Ground truth. (b) Euclidean distance based on feature vectors. (c–g) Different distances based on MFRCMs. (c) Manhattan. (d) Euclidean. (e) Wishart. (f) AIR. (g) GD. (h) Proposed GD-HWLKM.

processing. In the top of image shown in Fig. 5, the grayscale HH-polarization (HH-pol) SAR image overlaps on an optics image from Google Earth. It is obvious that this illuminated scene contains a part of urban region, river, farm land, asphalt roads, etc.

B. Experimental Result

1) Weighed Estimation Result of Coherency Matrix: An accurate false color image is an intuitionistic expression for different ground covers with polarimetric information, which is consist of multiple scattering components from different scattering

TABLE II
CLASSIFICATION ACCURACY (%) OF DIFFERENT METHODS

	Buildings	High-density vegetation	Low-density vegetation	Water	Bare soil	OA
Euclidean (pixel vector)	31.69	26.89	55.66	94.74	76.66	61.18
Manhattan	70.74	11.32	14.05	99.70	73.77	61.67
Euclidean	83.97	29.29	24.01	99.05	85.02	70.50
Wishart	63.48	86.44	84.39	93.25	23.59	75.47
AIR	84.97	93.24	64.74	99.28	44.69	83.52
GD	87.94	94.24	54.55	98.95	57.92	84.73
GD-HWLKM	86.82	92.56	73.74	99.19	80.97	89.78

TABLE III
AVERAGING RESIDUAL CNR AFTER CLUTTER SUPPRESSION

Polarization	Methods based on ADPCA processing	Averaging residual CNR(dB)		
		Extreme strong clutter	Urban area, such as buildings	Vegetation and bare soil,
HH	Before suppression	49.66	31.70	24.16
	Without classification	24.14	12.25	1.26
	With classification	6.70	2.03	1.35
HV	Before suppression	41.70	23.38	17.87
	Without classification	18.04	6.07	0.63
	With classification	7.30	1.23	0.35
VH	Before suppression	41.59	23.50	17.75
	Without classification	16.72	5.66	0.59
	With classification	6.19	1.53	0.62
VV	Before suppression	55.31	34.82	24.17
	Without classification	25.60	12.70	1.53
	With classification	8.61	2.84	1.55

mechanisms based on given decomposition theories. The false color images based on Yamaguchi decomposition are shown in Fig. 6(a) and (b), which are from the traditional estimated coherency matrix (we call it as "the traditional estimated method") and the proposed weighed estimated coherency matrix (we call it as "the proposed estimated method"), respectively. Due to the use of the simple averaging filter in one receiving channel, a large number of vegetation is mistakenly recognized as surface scatterings with the traditional estimated method. However, the proposed estimated method can increase the estimation accuracy of the coherency matrixes by the two steps, including a weighted multilook operator with the multipolarimetric data and the multichannel coherency matrix fusion using correlation coefficient. This method not only can take the similarity of pixels into consideration to avoid the over-smoothing problem, but also can fuse the coherency matrixes of different receiving channels to obtain a robust estimation value. To further quantitatively analyze the performance of the proposed method, the power contributions of different scatterings are shown in Fig. 6(c). It is obvious that the volume scattering component is enhanced from 30% to 51% and the double-bounce scattering component has a few decreases in a certain extent, which are the mistaken scatterings of the traditional estimated method.

2) Classification Result of PolSAR Image: To demonstrate the effectiveness of the proposed multichannel GD-HWLKM PolSAR classification approach, several classification methods within the K-mean cluster algorithm framework are shown in Fig. 7, which are based on different metrics, including Manhattan metric, Euclidean metric, Wishart metric, AIR metric, and GD metric. It should be noted that the different classifiers have the same inputs (coherency matrices, which are obtained
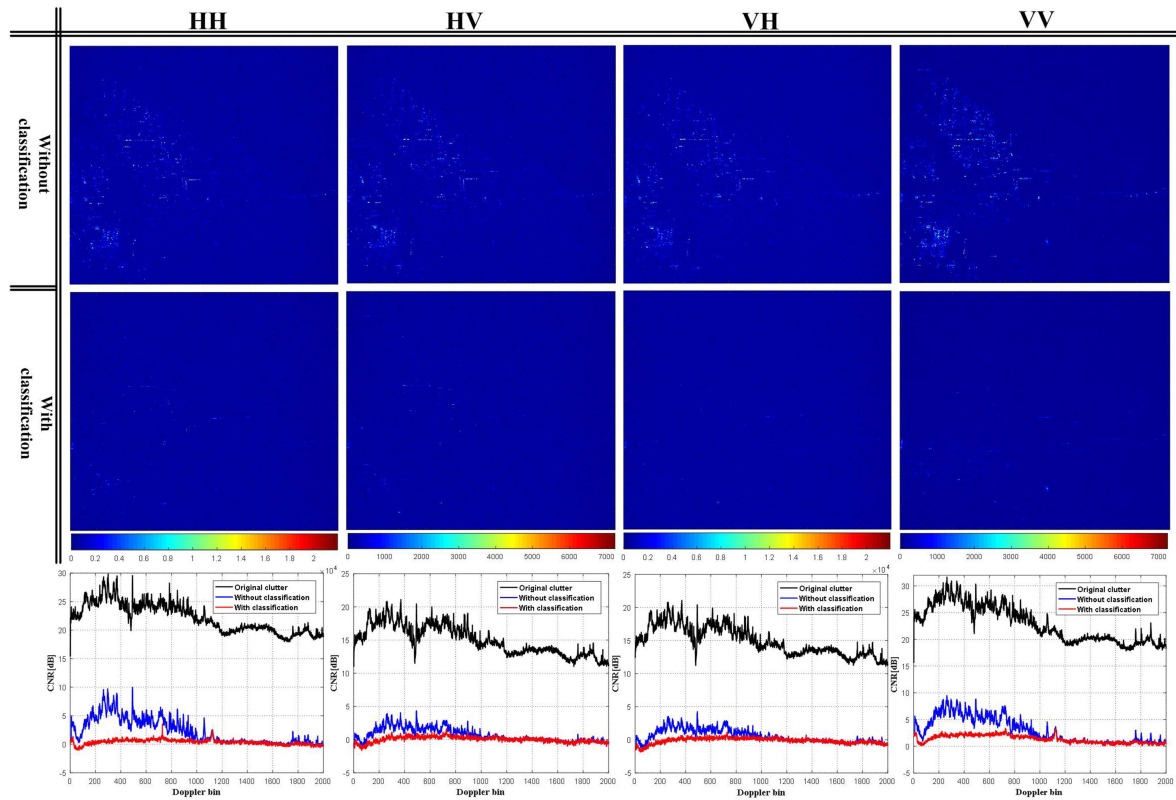
Fig. 8. Suppression residue without or with classification for different polarimetric channels (HH, HV, VH, VV), where the eight pictures at the top are the residual maps after clutter suppression and the four graphs at the bottom are the corresponding average power of all range bins.
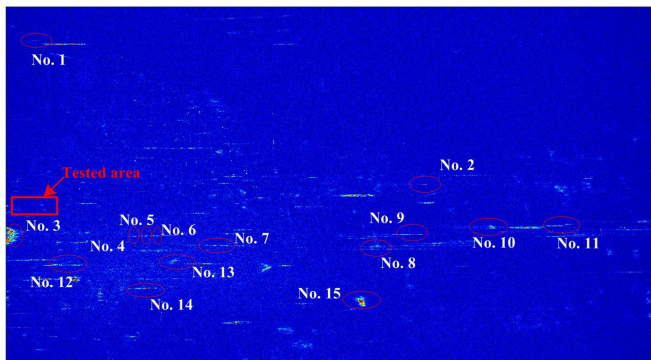

Fig. 9. Result of clutter suppression of VV-pol channel, where the red rectangle depicts the tested area in urban, and the 15 selected moving targets are labeled with white number.

by the proposed weighted estimation method). The ground truth is shown in Fig. 7(a), which is from the manual segmentation by the "Image Labeler" toolbox of MATLAB under the guidance of the Google Earth© optics image. There are five ground covers including buildings, high-density vegetation, low-density vegetation, water, and bare soil. Here, it should be specially pointed out that the roads will be divided into the water or bare soil category because they have similar scattering characteristics. In addition, some land covers located in the image border at the range direction will be also classified as the water, since they have the very low intensities with the influence of antenna pattern.

As shown in Table II, we can see that the proposed GD-HWLKM method shows superior classification results than other methods. It has the highest overall accuracy (OA) of 89.78% among all the methods. Fig. 7(c)–(h) show that the methods based on the MFRCMs can effectively suppress the speckle noise. Comparing the methods based on the MFRCMs, the method based on the pixel feature vectors has lots of small misclassified fragments on account of ignoring the spatial information, which results in the decrease of accuracy for all covers, as shown in Fig. 7(b). And, the classical methods based on norm-based metric have a relatively weak distinguishing ability for high-, or low-density vegetation, as shown in Fig. 7(c) and (d). The Wishart-based method can separate the different vegetation, but the classification accuracy of buildings is greatly reduced, as shown in Fig. 7(e). For the methods (AIR, GD) based on Riemannian space, as shown in Fig. 7(f) and (g), they can obtain a remarkable and great classification accuracy, since they can effectively tolerate the scaling or rotation between two MFRCMs and are more suitable to measure the similarity of matrixes. But, those methods usually cause smoothness of cover edges, which will lose a lot of edge information. Under this circumstance, it is very difficult that the roads are correctly classified. However, the proposed GD-HWLKM method not only takes the local spatial information into account by using GD to measure the similarity of MFRCMs, but also exploits three different types of weights (region-based weight, pixel-based weight, and local class distribution-based weigh) to describe the diversity among pixels from different scales, which can
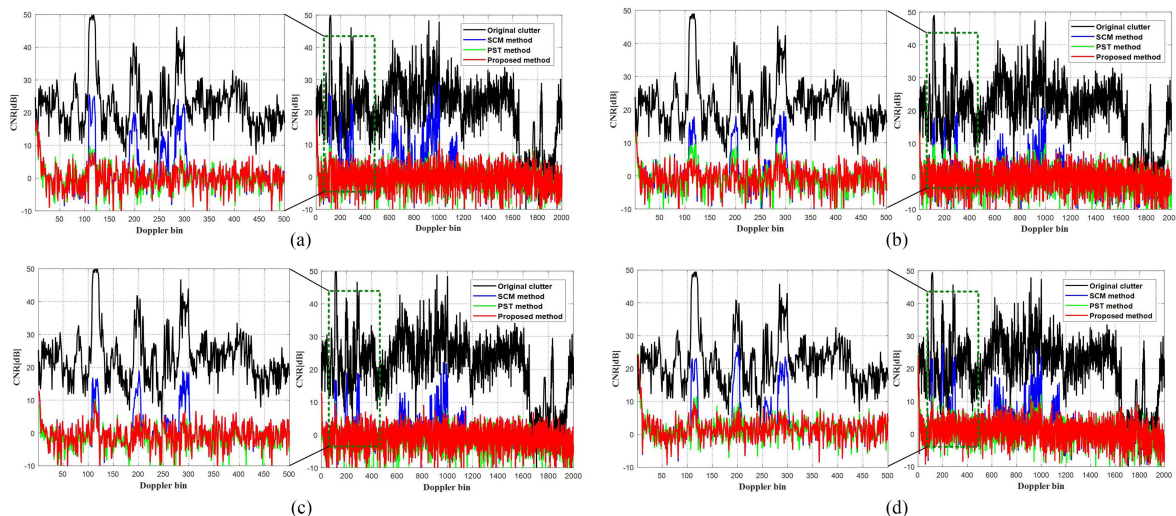
Fig. 10.   Results of clutter suppression without and with guidance of the classification. (a) HH-pol. (b) HV-pol. (c) VH-pol. (d) VV-pol channels.
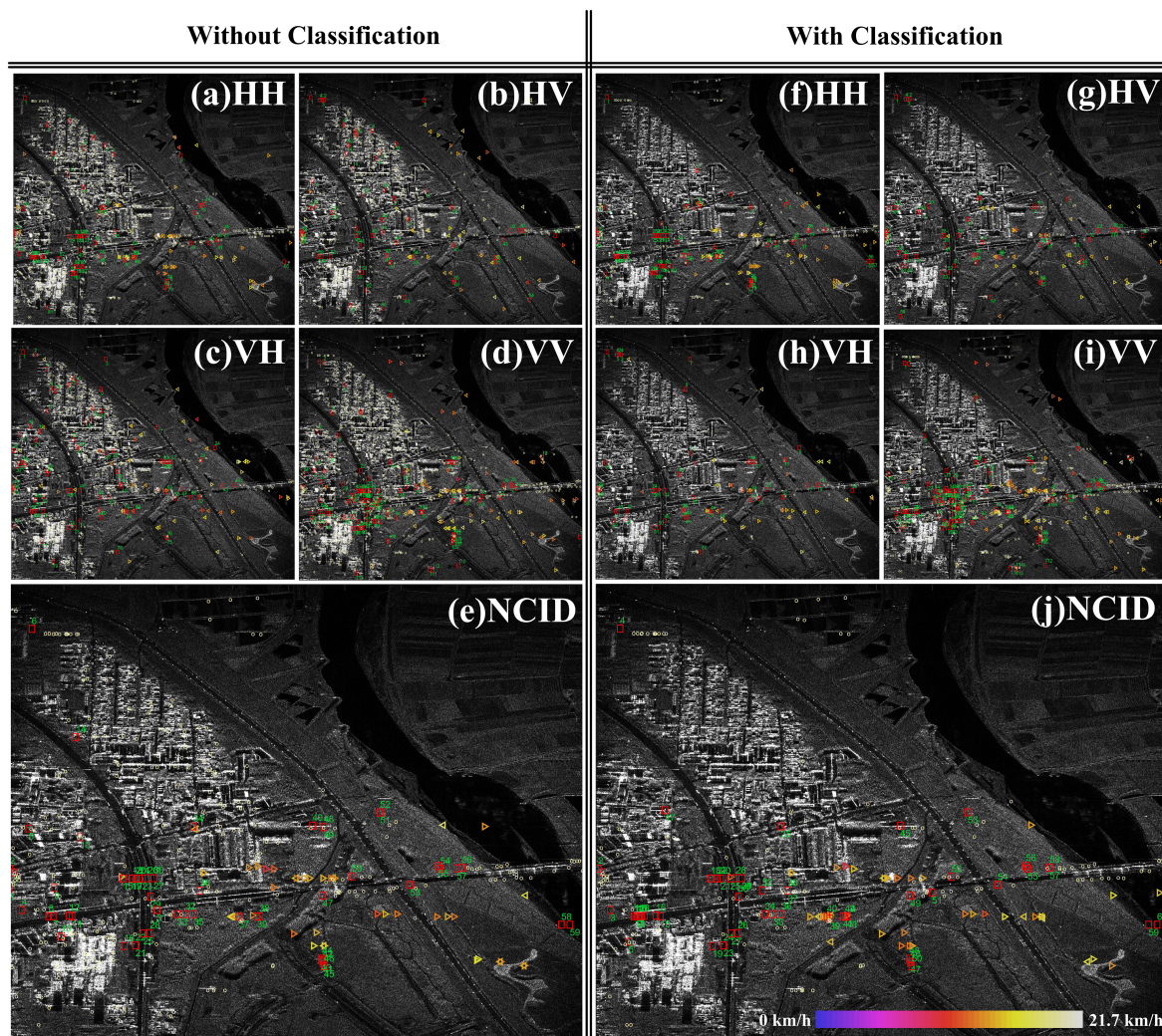

Fig. 11.   GMTI results without and with guidance of the classification for different polarization channels, where the single polarization channel with PFA $= 10^{-5}$ and the NCID with 2/4 rule with final PFA $= 6 \times 10^{-10}$. (a–e) are results without classification (a) HH-pol, (b) HV-pol, (c) VH-pol, (d) VV-pol, and (e) NCID. (f–j) are results with classification (f) HH-pol, (g) HV-pol, (h) VH-pol, (i) VV-pol, and (j) NCID. The false alarms are marked with yellow circles, the true moving targets are marked with red rectangles, and the triangle arrows represent the relocated positions of the detected targets with estimated cross-track velocities whose absolute values are denoted by different colors, as shown in the color bar on the bottom.
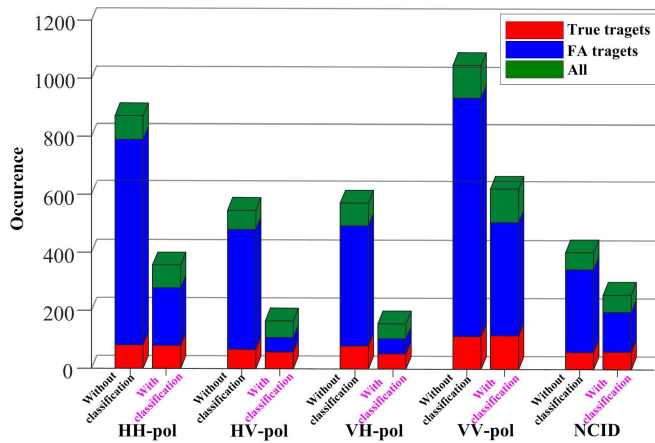
Fig. 12. Detection results for different processing without and with guidance of the classification.
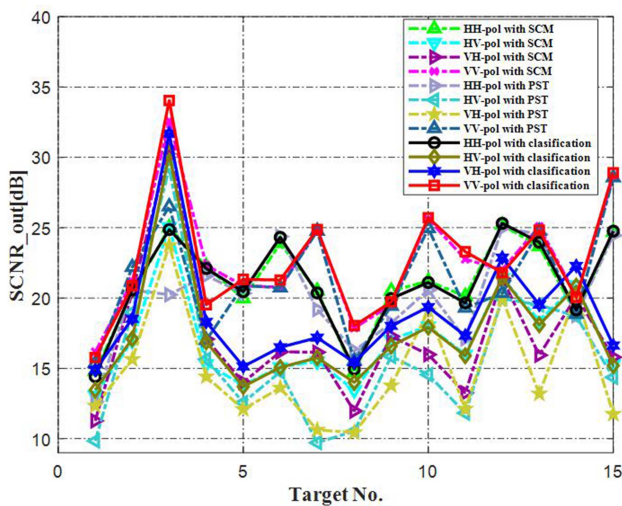

Fig. 13. Output SCNR of selected 15 moving targets without (SCM and PST) and with guidance of the classification for different polarization channels.

preserve the edges as many as possible. Furthermore, with the K-means algorithm framework, the proposed method can obtain unsupervised classification results with higher overall accuracy.

3) GMTI Processing Result: Under the guidance of polarimetric classification results (online knowledge), the accurate CCMs can be estimated for different ground covers, which can greatly improve the clutter suppression performance, especially for the strong clutter. Fig. 8 gives the suppression results of different polarimetric channels without classification (by SCM method) or with classification and the corresponding average power of all range bins. Intuitively, it can be found that the residual power of the urban area is less when using the classification information. To further quantitatively analyze the performance of the proposed method, the averaging residual CNR of different areas are calculated as listed in Table III, including extreme strong clutter, buildings, and natural scene such vegetation and bare soil. It is shown that the extreme strong clutter can be better suppression up to 11–17 dB and the averaging residual CNR of buildings is reduced by 4–10 dB. Furthermore, an urban area

marked by red rectangle is selected in Fig. 9 to compare clutter suppression performance with different CCM estimation methods for extreme strong clutter, as shown in Fig. 10. Here, SCM and PST methods are performed without any knowledge. As we can see, comparing the SCM method, the clutter suppression performance of the proposed method can be improved about 10–18 dB for different polarimetric channels. In addition, there also is a certain improvement about clutter cancellation ability besides the PST method because the used training samples are from the same land cover.

To further demonstrate the improvement of GMTI performance of the proposed method, we carry out the moving targets detection and parameter estimation for four polarimetric channels with or without classification result assistance, respectively. The GMTI results are shown in Fig. 11(a)–(d) and (f)–(i) with $PFA = 10^{-5}$ for different S-pol components, including HH-pol, HV-pol, VH-pol, and VV-pol channel. From Fig. 11(a)–(d), without classification results, it can be found that there are a large number of false alarms in urban area because of the residual power of strong clutter after cancellation, which are marked with yellow circles. Obviously, the proposed method can greatly reduce the false alarms and reserve the truth moving targets as much as possible, as shown in Fig. 11(f)–(i). Fig. 12 gives the number of detected targets (all, false alarm (FA), and true) from different processing methods. It should be noted that there are no cooperative targets in the experimental scene, so we distinguish the truth targets from all detected targets by the estimated velocity of targets and others are recognized as false alarm. In this article, the velocity threshold is set as 1.78 m/s, which is corroding to the 1/2 antenna beam main lobe.

In addition, to further improve the GMTI performance, we take advantage of NCID technique to combine the target-detection results of four S-pol channels. Although the scattering characteristics and power of targets and clutter are different between different polarimetric channels, they still can be considered as independent observations at the same time and the targets are more believable after NCID processing. In this article, the NCID technique is achieved by M/N rule (M = 2, N = 4) and the final $PFA = 6 \times 10^{-10}$. The detection results of 2/4 rule without or with classification information are demonstrated in Fig. 11(d) and (j), respectively. And the number of detected targets is shown in Fig. 12. Evidently, the NCID technique can improve the detection performance, further. Specifically, the most of true moving targets are effectively preserved when remarkably reducing the false alarms in urban area. Additionally, 15 moving targets are selected to compare the improvement of output SCNR. The locations of selected targets are marked in Fig. 9 and their SCNRs are depicted in Fig. 13 for different polarimetric channels with different methods, including SCM, PST, and the proposed method. As it can be seen more clearly, comparing the results with SCM and PST methods, the output SCNRs for most of the targets are improved, because the over-estimation problem of CCM almost is almost avoided under the guidance of the previous classification results. In summary, the proposed method can improve the GMTI performance in evident reduction of the false alarms and the improvement of moving-target detection performance.

V. Conclusion

An online Pol-KA SAR-GMTI approach has been proposed in this article to improve the GMTI performance by online polarization classification result, which need not any prior knowledge and can suit the complicated geographical environment. For obtaining the online knowledge, the weighed estimation of coherency matrix with the multichannel SAR system, the multiple feature extraction with RCMs, and the unsupervised classification by the proposed GD-HWLKM clustering algorithm is performed in sequence. Typically, the proposed weighed estimation method of coherency matrix makes full use of the spatial information by fusing the coherency matrixes from different azimuth receive channels in multichannel. And the proposed unsupervised GD-HWLKM PolSAR image clustering approach can achieve a better classification performance when preserving the edges. Under the guidance of the online knowledge, the IID clutter training samples are selected to accurately estimate the CCMs of different land covers, which can improve suppression performance about 10–18 dB and detection performance moving targets on the decrease of the false alarms and the increase of output SCNR of moving targets. In addition, we perform the SAR-GMTI processing for HH-, HV-, VH-, and VV-pol components, respectively. How to joint polarimetric and spatial adaptive processing for GMTI with the guidance of online knowledge will be under investigation in our future work to achieve the better improvement performance of clutter suppression and moving-target detection.
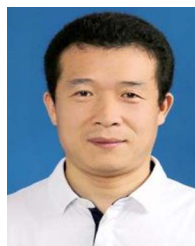
Acknowledgment

References

[1] P. Lombardo, F. Colone, and D. Pastina, "Monitoring and surveillance potentialities obtained by splitting the antenna of the COSMO-SkyMed SAR into multiple sub-apertures," *IEEE Proc. Radar Sonar Navigation*, vol. 153, no. 2, pp. 104–116, May 2006.

[2] D. Cerutti-Maori, J. Klare, and A. R. Brenner, "Wide-region traffic monitoring with the SAR/GMTI system PAMIR," *IEEE Trans. Geosci. Remote Sens.*, vol. 46, no. 10, pp. 3019–3030, Oct. 2008.

[3] D. Cerutti-Maori, I. Sikaneta, and C. H. Gierull, "Optimum SAR/GMTI processing and its application to the radar satellite RADARSAT-2 for traffic monitoring," *IEEE Trans. Geosci. Remote Sens.*, vol. 50, no. 10, pp. 3868–3881, Oct. 2012.

[4] E. Makhoul, S. V. Baumgartner, M. Jäger, and A. Broquetas, "Multichannel SAR-GMTI in maritime scenarios with F-SAR and terraSAR-X sensors," *IEEE J. Sel. Topics Appl. Earth Observ. Remote Sens.*, vol. 8, no. 11, pp. 5052–5067, Nov. 2015.

[5] X. Liu et al., "A comparison to joint pixel vector methods for clutter suppression in SAR-GMTI system," in *Proc. 12th Int. Conf. Signal Process.*, 2014, pp. 2039–2043.

[6] I. S. Reed, J. D. Mallett, and L. E. Brennan, "Rapid convergence rate in adaptive arrays," *IEEE Trans. Aerosp. Electron. Syst.*, vol. AES-10, no. 6, pp. 853–863, Nov. 1974.

[7] D. J. Rabideau and A. O. Steinhardt, "Improved adaptive clutter cancellation through data-adaptive training," *IEEE Trans. Aerosp. Electron. Syst.*, vol. 35, no. 3, pp. 879–891, Jul. 1999.

[8] M. C. Wicks, M. Rangaswamy, R. Adve, and T. B. Hale, "Space-time adaptive processing: A knowledge-based perspective of airborne radar," *IEEE Trans. Signal Process.*, vol. 23, no. 1, pp. 56–61, Jan. 2006.

[9] E. Conte, A. Demaio, A. Farina, and G. Foglia, "Design and analysis of a knowledge-aided radar detector for doppler processing," *IEEE Trans. Aerosp. Electron. Syst.*, vol. 42, no. 3, pp. 1058–1079, Jul. 2006.

[10] X. Zhu, J. Li, and P. Stoica, "Knowledge-aided space-time adaptive processing," *IEEE Trans. Aerosp. Electron. Syst.*, vol. 47, no. 2, pp. 1325–1333, Apr. 2011.

[11] O. Harant et al., "Fisher PDF for maximum likelihood texture tracking with high resolution PolSAR data," in *Proc. 8th Eur. Conf. Synth. Aperture Radar*, 2010, pp. 1–4.

[12] X. Liu, L. Jiao, X. Tang, Q. Sun, and D. Zhang, "Polarimetric convolutional network for PolSAR image classification," *IEEE Trans. Geosci. Remote Sens.*, vol. 57, no. 5, pp. 3040–3054, May 2019.

[13] J. Cheng, F. Zhang, D. Xiang, Q. Yin, and Y. Zhou, "PolSAR image classification with multiscale superpixel-based graph convolutional network," *IEEE Trans. Geosci. Remote Sens.*, vol. 60, 2022, Art. no. 5209314, doi: 10.1109/TGRS.2021.3079438.

[14] D. Guan, D. Xiang, X. Tang, L. Wang, and G. Kuang, "Covariance of textural features: A new feature descriptor for SAR image classification," *IEEE J. Sel. Topics Appl. Earth Observ. Remote Sens.*, vol. 12, no. 10, pp. 3932–3942, Oct. 2019.

[15] H. Liu, F. Wang, S. Yang, B. Hou, L. Jiao, and R. Yang, "Fast semisupervised classification using histogram-based density estimation for large-scale polarimetric SAR data," *IEEE Trans. Geosci. Remote Sens. Lett.*, vol. 16, no. 12, pp. 1844–1848, Dec. 2019.

[16] A. Blum and T. Mitchell, "Combining labeled and unlabeled data with co-training," in *Proc. 11th Annu. Conf. Comput. Learn. Theory*, 1998, pp. 92–100.

[17] H. Liu et al., "Fast semi-supervised classification based on parallel auction graph for polarimetric SAR data," in *Proc. IEEE Int. Geosci. Remote Sens. Symp.*, 2016, pp. 1528–1531.

[18] H. Liu, Y. Wang, S. Yang, S. Wang, J. Feng, and L. Jiao, "Large polarimetric SAR data semi-supervised classification with spatial-anchor graph," *IEEE J. Sel. Topics Appl. Earth Observ. Remote Sens.*, vol. 9, no. 4, pp. 1439–1458, Apr. 2016.

[19] J. S. Lee, M. R. Grunes, T. L. Ainsworth, L. J. Du, D. L. Schuler, and S. R. Cloude, "Unsupervised classification using polarimetric decomposition and the complex Wishart classifier," *IEEE Trans. Geosci. Remote Sens.*, vol. 37, no. 5, pp. 2249–2258, Sep. 1999.

[20] Y. Wu, K. Ji, W. Yu, and Y. Su, "Region-based classification of polarimetric SAR images using Wishart MRF," *IEEE Geosci. Remote Sens. Lett.*, vol. 5, no. 4, pp. 668–672, Oct. 2008.

[21] A. P. Doulgeris, "An automatic u-distribution and Markov random field segmentation algorithm for PolSAR images," *IEEE Trans. Geosci. Remote Sens.*, vol. 53, no. 4, pp. 1819–1827, Apr. 2015.

[22] J.-S. Lee, M. R. Grunes, E. Pottier, and L. Ferro-Famil, "Unsupervised terrain classification preserving polarimetric scattering characteristics," *IEEE Trans. Geosci. Remote Sens.*, vol. 42, no. 4, pp. 722–731, Apr. 2004.

[23] L. Ferro-Famil, E. Pottier, and J. S. Lee, "Unsupervised classification of multifrequency and fully polarimetric SAR images based on the H/A/Alpha Wishart classifier," *IEEE Trans. Geosci. Remote Sens.*, vol. 39, no. 11, pp. 2332–2342, Nov. 2001.

[24] P. R. Kersten, J. S. Lee, and T. L. Ainsworth, "Unsupervised classification of polarimetric synthetic aperture radar images using fuzzy clustering and EM clustering," *IEEE Trans. Geosci. Remote Sens.*, vol. 43, no. 3, pp. 519–527, Mar. 2005.

[25] J. S. Lee, M. R. Grunes, and R. Kwok, "Classification of multi-look polarimetric SAR imagery based on the complex Wishart distribution," *Int. J. Remote Sens.*, vol. 15, no. 11, pp. 2299–2311, 1994.

[26] Q. Chen, G. Kuang, J. Li, L. Sui, and D. Li, "Unsupervised land cover/land use classification using PolSAR imagery based on scattering similarity," *IEEE Trans. Geosci. Remote Sens.*, vol. 51, no. 3, pp. 1817–1825, Mar. 2013.

[27] H. Bi, J. Sun, and Z. Xu, "Unsupervised PolSAR image classification using discriminative clustering," *IEEE Trans. Geosci. Remote Sens.*, vol. 55, no. 6, pp. 3531–3544, Jun. 2017.

[28] O. Tuzel, F. Porikli, and P. Meer, "Region covariance: A fast descriptor for detection and classification," in *Computer Vision-ECCV*. Berlin, Germany: Springer-Verlag, 2006, pp. 589–600.

[29] M.-T. Pham, G. Mercier, and J. Michel, "PW-COG: An effective texture descriptor for VHR satellite imagery using a pointwise approach on covariance matrix of oriented gradients," *IEEE Trans. Geosci. Remote Sens.*, vol. 54, no. 6, pp. 3345–3358, Jun. 2016.

[30] R. Hathaway, J. Bezdek, and Y. Hu, "Generalized fuzzy c-means clustering strategies using norm distances," *IEEE Trans. Fuzzy Syst.*, vol. 8, no. 5, pp. 576–582, Oct. 2000.

[31] L. Bobrowski and J. Bezdek, "C-means clustering with the and norms," *IEEE Trans. Syst., Man, Cybern.*, vol. 21, no. 3, pp. 545–554, May/Jun. 1991.

[32] V. Arsigny, P. Fillard, X. Pennec, and N. Ayache, "Log-Euclidean metrics for fast and simple calculus on diffusion tensors," *Magn. Reson. Med.*, vol. 56, no. 2, pp. 411–421, 2006.

[33] H. Song, W. Yang, Y. Bai, and X. Xu, "Unsupervised classification of polarimetric SAR imagery using large-scale spectral clustering with spatial constraints," *Int. J. Remote Sens.*, vol. 36, no. 11, pp. 2816–2830, 2015.

[34] M.-T. Pham, "Fusion of polarimetric features and structural gradient tensors for VHR PolSAR image classification," *IEEE J. Sel. Topics Appl. Earth Observ. Remote Sens.*, vol. 11, no. 10, pp. 3732–3742, Oct. 2018.

[35] L. Jing, M. Ng, and Z. Huang, "An entropy weighting k-means algorithm for subspace clustering of high-dimensional sparse data," *IEEE Trans. Knowl. Data Eng.*, vol. 19, no. 8, pp. 1026–1041, Aug. 2007.

[36] C.-Y. Tsai and C.-C. Chiu, "Developing a feature weight self-adjustment mechanism for a k-means clustering algorithm," *Comput. Statist. Data Anal.*, vol. 52, no. 10, pp. 4658–4672, 2008.

[37] D. Xiang, T. Tang, S. Quan, D. Guan, and Y. Su, "Adaptive superpixel generation for SAR images with linear feature clustering and edge constraint," *IEEE Trans. Geosci. Remote Sens.*, vol. 57, no. 6, pp. 3873–3889, Jun. 2019.

[38] D. Ratha, S. De, T. Celik, and A. Bhattacharya, "Change detection in polarimetric SAR images using a geodesic distance between scattering mechanisms," *IEEE Geosci. Remote Sens. Lett.*, vol. 14, no. 7, pp. 1066–1070, Jul. 2017.

[39] D. Ratha, A. Bhattacharya, and A. C. Frery, "Unsupervised classification of PolSAR data using a scattering similarity measure derived from a geodesic distance," *IEEE Geosci. Remote Sens. Lett.*, vol. 15, no. 1, pp. 151–155, Jan. 2018.

[40] A. Liu, F. Wang, H. Xu, and L. Li, "N-SAR: A new multi-channel multimode polarimetric ariborne SAR," *IEEE J. Sel. Topics Appl. Earth Observ. Remote Sens.*, vol. 11, no. 9, pp. 3155–3166, Sep. 2018.

[41] C. Han, Z. Yang, Q. Zhang, P. Huang, and H. Xu, "A multifeature TDAO-AIR clutter classification approach for inshore ambiguity identification and suppression with azimuth multichannel SAR system," *IEEE Trans. Geosci. Remote Sens.*, vol. 60, 2022, Art. no. 5206215, doi: 10.1109/TGRS.2021.3072313.

[42] L. Sachs, *Applied Statistics: A Handbook of Techniques*. Berlin, Germany: Springer, 2012.

[43] Y. Yamaguchi, A. Sato, W.-M. Boerner, R. Sato, and H. Yamada, "Four-component scattering power decomposition with rotation of coherency matrix," *IEEE Trans. Geosci. Remote Sens.*, vol. 49, no. 6, pp. 2251–2258, Jun. 2011.

[44] S. R. Cloude and E. Pottier, "A review of target decomposition theorems in radar polarimetry," *IEEE Trans. Geosci. Remote Sens.*, vol. 34, no. 2, pp. 498–518, Mar. 1996.

[45] S. Uhlmann and S. Kiranyaz, "Integrating color features in polarimetric SAR image classification," *IEEE Trans. Geosci. Remote Sens.*, vol. 52, no. 4, pp. 2197–2216, Apr. 2014.

[46] E. J. Rignot and J. J. V. Zyl, "Change detection techniques for ERS-SAR data," *IEEE Trans. Geosci. Remote Sens.*, vol. 31, no. 4, pp. 896–906, Jul. 1993.

[47] W. Du, Z. Yang, and G. Liao, "Improved ground moving target indication method in heterogeneous environment with polarization-aided adaptive processing," *IEEE Geosci. Remote Sens. Lett.*, vol. 13, no. 11, pp. 1729–1733, Nov. 2016.

Zhiwei Yang was born in Sichuan, China, in 1980. He received the M.S. and Ph.D. degrees in electrical engineering from Xidian University, Xi'an, China, in 2005 and 2008, respectively.

He is currently a Full Professor with the National Laboratory of Radar Signal Processing, Xidian University. He has authored or coauthored more than 100 papers. Moreover, he designed the ground moving target indication algorithms for the space-borne SAR/GMTI systems in China. His research interests include adaptive array signal processing, space-time-polarmetric adaptive processing, air-borne/space-borne moving target indication and imaging, multidimensional signal processing, and sparse signal processing.

Guisheng Liao (Senior Member, IEEE) was born in Guiling, China. He received the B.S. degree in science from Guangxi University, Guangxi, China, in 1985, and the M.S. and Ph.D. degrees in electrical engineering from Xidian University, Xi'an, China, in 1990 and 1992, respectively.

He is currently a Professor with Xidian University, where he is also the Dean of the School of Electronic Engineering. He has been a Senior Visiting Scholar with the Chinese University of Hong Kong, Hong Kong. His research interests include synthetic aperture radar (SAR), space–time adaptive processing, SAR ground moving target indication, and distributed small satellite SAR system design.

Prof. Liao is a Member of the National Outstanding Person and the Cheung Kong Scholars in China.

Qingjun Zhang was born in Jiangsu, China, in 1969. He received the M.S. degree in automation of electrical power system from North China Electric Power University, Beijing, China, in 1993.

He is currently the Chief Designer and Chief Commander of satellite design and space remote sensing field in China. His research interests include satellite system design and microwave remote sensing technology.

Shun He was born in Hunan, China, in 1980. She received the B.S. degree in communication engineering from Guilin University of Electronic Technology, Guilin, China, in 2005, and the Ph.D. degree in electrical engineering from the National Laboratory of Radar Signal Processing, Xidian University, Xi'an, China, in 2016.

Her current research interests include adaptive array signal processing, wideband signal processing.

Chaolei Han was born in Henan, China, in 1993. He received the B.S. degree in electrical engineering in 2017 from Xidian University, Xi'an, China, where he is currently working toward the Ph.D. degree with the National Laboratory of Radar Signal Processing.

His research interests include synthetic aperture radar, space-time adaptive processing, ground moving target indication, space-time-polarmetric adaptive processing, and multidimensional signal processing.

Huajian Xu was born in Fujian, China, in 1990. He received the B.S. and Ph.D. degrees in electrical engineering from Xidian University, Xi'an, China, in 2013 and 2018, respectively.

He is currently with Nanjing Electronic Equipment Institute, Nanjing, China. He is mainly engaged in the design of passive location system. His research interests include synthetic aperture radar, ground moving target indication, and space-time adaptive processing.